Reaction Phenomena in a Nonthermal Equilibrium Plasma

John B. Gustafson
Antony N. Beris
Henry C. Foley
Department of Chemical Engineering
University of Delaware
Newark, DE 19716

An exact description of a plasma is given by the well-known Boltzmann kinetic equation, which governs the time evolution of the species energy distribution function, $f_i(\rho \mathbf{v}, \mathbf{r}, t)$, in six-dimensional phase space and time (Chung et al., 1975). However, the solution of this equation is not tractable for other than a few simplified cases because of the high dimensionality and the need for information on the discrete particle interactions (Kline and Kushner, 1989). Thus, simulations of the plasmas, glow discharges, used in plasma-assisted chemical reactors, are typically based on assumed forms of the species energy distributions. An example is the continuum approximation (Graves, 1986), which is derived by taking the moments of the kinetic equation and by integrating over velocity space, assuming a Maxwell-Boltzmann (MB) form for the species energy distributions. The MB form of the distribution function implies thermal equilibrium which, under the conditions used for glow discharges, might not be established among the electrons. The electron energy distribution function, EEDF, is a function of both space and time and may deviate significantly from the thermal MB distribution. Recently, Monte Carlo (Kushner, 1988; Kline et al., 1989), kinetic (Sommerer et al., 1989), and particle-in-cell (Boswell and Morey, 1987) methods have been used to address the nonequilibrium nature of the electron energy distribution in plasma simulations.

The deviation of the EEDF from an MB distribution has been examined by Shirai and Tabei (1986), who matched predicted and experimental spectroscopic measurements in a DC nitrogen discharge. Langmuir probe measurements of the EEDF in a radio frequency (RF) generated argon plasma by Cox et al. (1987) and Deshmukh and Cox (1988) have shown that the EEDF typically deviates from the thermal MB form and that the deviation from thermal equilibrium increases at low pressure. This observation is complemented by the theoretical work of Loureiro and Ferreira (1989); Ferreira and Loureiro, 1988), who solved a simplified, homogeneous form of the Boltzmann kinetic equation for a nitrogen plasma. They showed that when the excitation frequency is increased relative to the electron–neutral collision frequency, the number of high-energy electrons in the tail of the EEDF approaches the thermal MB distribution. The variation in the EEDF due to collisions of electrons with molecular and atomic species, which result in electronic and vibrational excitations, has been theoretically investigated in various RF-generated plasmas by Capitelli et al. (1987, 1988). In general, the electronic and vibrational excitation reactions lead to a reduction in the density of electrons with energies above the excitation threshold energies. Wani (1988) has shown that the introduction of even small amounts of mercury into an argon plasma significantly alters the EEDF above the mercury ionization threshold energy.

Spatial variations in the EEDF were measured experimentally in the cathode of an RF-generated hydrogen plasma by Boyd and Twiddy (1959). More recently, various researchers (Kushner, 1983; Boeuf and Marode, 1982; Ohuchi and Kubota, 1983) have examined theoretically the variation of the EEDF across the cathode sheath, using Monte Carlo simulations. These studies show that electrons are generated at the cathode and then are accelerated into the glow across the sheath by the electric field. Thus, the EEDF is approximately monoenergetic near the cathode and then gradually disperses, through collisions with heavy species, toward a more or less thermal distribution as the sheath–glow boundary is approached.

There is experimental evidence in the literature that the performance of a plasma reactor is affected by changes in the EEDF. In a review article, Wertheimer and Moisan (1985) attributed the alteration in reactor performance, produced by changes in excitation frequency, to changes in the EEDF in the glow. Specifically, they suggest that observed changes in deposition or etching rates result from variations in the concentration of the reactive species due to the alteration of the number density of electrons in the high-energy tail of the EEDF. For

Correspondence concerning this paper should be addressed to A. N. Beris.

example, the several orders of magnitude increase in etching rate of an organic photoresist by a microwave-generated oxygen plasma as compared to that observed in a RF-generated plasma, corresponded to a measurable increase in the oxygen atom concentration, and was attributed to an increase in the density of the high energy tail of the EEDF. This note addresses, with theoretical simulations, the extent to which the EEDF plays a role in the reaction kinetics of the plasma.

EEDF and Reaction Rate Constants

The impact of the EEDF on the bulk reaction rates can be visualized by considering the calculation of the rate constants, k_j, using the kinetic theory expression:

$$k_j = \int_{E_{th,j}}^{\infty} \left(\frac{2\epsilon}{m_i}\right) f_j(\epsilon)\sigma_j(\epsilon)\, d\epsilon \tag{1}$$

where ϵ is the collision energy, and $f_j(\epsilon)$, $\sigma_j(\epsilon)$, and $E_{th,j}$ are respectively the collision energy distribution, the collision cross section, and the threshold energy for reaction j. In the collision of a heavy ion or neutral particle with an electron the energy of the heavy particle can be neglected, since in a glow discharge it is typically several orders of magnitude lower than that of the electron. Thus, for these reactions, the collision energy distribution is simply the electron energy distribution, EEDF, and their relative rates depend on the product of their respective collision cross sections and the EEDF.

In order to quantify the effect of changes in the EEDF on the reaction rates, we have developed a prototype reaction simulation for a hydrogen plasma that is not diffusion limited. Our work follows that of Fukumasa et al. (1985), who modeled a magnetic multipole ion source. We consider the following species: electrons (e), molecular hydrogen (H_2), atomic hydrogen (H), and the associated ions (H^+, H_2^+, and H_3^+). The homogeneous steady state reaction model for the evolution of the ith species number density, n_i, is given by:

$$\frac{dn_i}{dt} = \sum_{j=1}^{M} (x_{i,j} r_j) - n_i k_{\text{loss},i} = 0 \tag{2}$$

where the rate of reaction j is given by

$$r_j = k_j n_e^{Ze,j} n_{H_2}^{Z_{H_2,j}} \prod_{i=1}^{N} n_i^{Z_{i,j}} \tag{3}$$

and $z_{e,j}$, $z_{H_2,j}$, and $z_{i,j}$ are the reactant stoichiometric coefficients

Table 1. Reaction Network—Hydrogen Plasma

Reaction	Threshold Energy eV
$H + e \Rightarrow H^+ + 2e$	13.6
$H^+ + e \Rightarrow H + h\nu$	<13.6
$H_2 + e \Rightarrow H_2^+ + 2e$	15.4
$H_2 + e \Rightarrow 2H + e$	10.0
$H_2 + e \Rightarrow H + H^+ + e$	18.0
$H_2 + H^+ \Rightarrow H_2^+ + H$	1.8
$H_2^+ + e \Rightarrow H + H^+ + e$	2.4
$H_2^+ + e \Rightarrow 2H$	0.0
$H_2^+ + H_2 \Rightarrow H_3^+ + H$	0.0
$H_3^+ + e \Rightarrow H_2 + H$	0.0
$H_3^+ + e \Rightarrow 2H + H^- + 2e$	14.0
$H_3^+ + e \Rightarrow 3H$	0.0

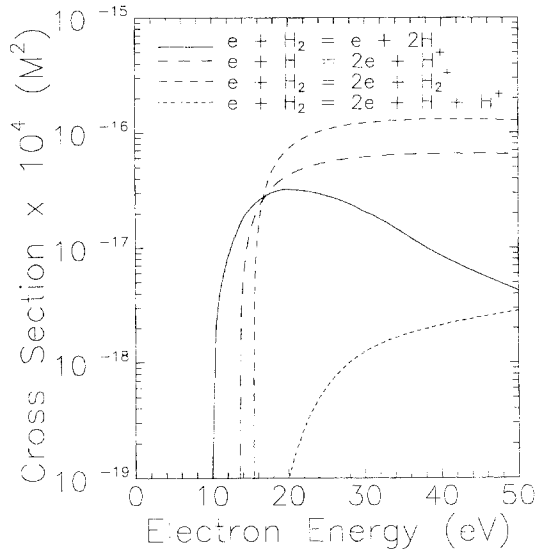

Figure 1. Collision cross-sections for several example reactions.

of the species e, H_2, and i, respectively, in reaction j, and $x_{i,j}$ is the net stoichiometric coefficient (product–reactant) of species i in reaction j. The above equations are solved for all species densities except for the electron and hydrogen molecule densities, which are fixed by charge and hydrogen atom conservation, respectively, given by:

$$n_e = \sum_{i=1}^{N} y_{e,i}\, n_i \tag{4}$$

$$n_{H_2} = n_{H_2}^0 - \sum_{i=1}^{N} \frac{1}{2} y_{H,i}\, n_i \tag{5}$$

where $y_{e,i}$ and $y_{H,i}$ are the net charge and number of H atoms in species i, respectively, and $n_{H_2}^0$ is the initial hydrogen density.

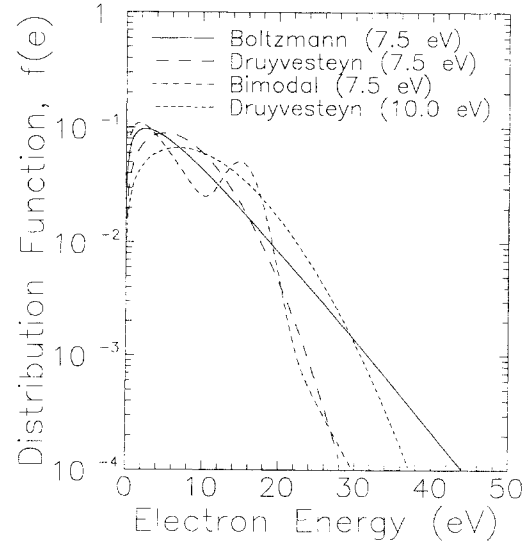

Figure 2. Electron energy distributions.

Table 2. Results Obtained with Different Maxwell-Boltzmann Electron Beam Bimodal Distributions

kT, eV	5.0	5.0	5.0	5.0	5.0	5.0	5.0	5.0
Fraction normal beam	0.0	0.15	0.15	0.15	0.15	0.15	0.15	0.15
Beam average energy, eV	0.0	10.0	12.5	13.5	15.0	17.0	19.0	20.0
Net average energy, eV	7.5	7.9	8.3	8.4	8.6	8.9	9.2	9.4
Fractional ionization $\times 10^3$	3.8	1.8	1.9	2.0	2.0	2.3	3.6	7.3
H, as fraction of TI*	2.74	2.40	3.46	3.94	3.73	3.59	3.80	4.20
H^-, as fraction of TI*	0.14	0.08	0.08	0.08	0.08	0.09	0.15	0.27
H_2^+, as fraction of TI*	0.21	0.20	0.20	0.20	0.20	0.20	0.21	0.22
H_3^+, as fraction of TI*	0.65	0.72	0.72	0.72	0.72	0.71	0.64	0.50

*TI = total ionization

For simplicity we have assumed that all species other than H_2 recombine at the wall to form H_2 with a rate constant given by the inverse of the corrected average time required for the species to reach the reactor wall, as predicted by the kinetic theory of gases.

$$k_{\text{loss},i} = \tau_i^{-1}; \quad \tau_i = \frac{4}{\gamma_i}\frac{V}{A}\left(\frac{3m_i}{kT_i}\right)^{1/2} \tag{6}$$

where the kinetic velocity of the species is given by $(3m_i/kT_i)^{1/2}$, and the volume to area ratio of the reactor vessel is given by V/A. The transition time includes an empirical correction factor, γ_i, that accounts for the recombination or reaction probability at the wall. The values for γ_i used in this work are 0.1 for the hydrogen atoms and 0.057 for the ionic species. These values were taken from the base case of Fukumasa et al. (1985), which was fitted to experimental data. The complete reaction network used in this simulation, including ionization of H_2 and H, and dissociation of H_2 and H_2^+ and photorecombination, along with the corresponding threshold energies, is given in Table 1. Several typical collision cross sections, obtained from the literature (Janev et al., 1987), are plotted in Figure 1. The significant attributes of the cross sections are the threshold energies, above which the cross sections obtain a finite value, the location and magnitude of the maximum of the cross sections, and the high-energy decay of the cross section.

Forms of the EEDF

The EEDF can deviate significantly from the thermal equilibrium Maxwell-Boltzmann distribution. In our analysis, we considered three basic forms of the EEDF, a Maxwell-Boltzmann distribution, a Druyvesteyn distribution, and a bimodal distribution based on the experimental results of Deshmukh and Cox (1988). Typical example distributions are shown in Figure 2.

The MB distribution is consistent with thermal equilibrium and assumes that the energy gained by the electron from the imposed electric field is randomly redistributed by means of electron–electron interactions (Venugopalan, 1971). It is an appropriate distribution for a plasma at high densities and low applied electric fields, when the electrons quickly approach equilibrium. On the other hand, the Druyvesteyn distribution assumes that the gain of energy by the electrons from the imposed electric field is balanced entirely by elastic collisions with heavy species so that the fractional energy loss and the mean free path between collisions is constant at all energies (Venugopalan, 1971). This distribution is most likely when the lowest excitation threshold energy for all species in the plasma is significantly greater than the average electron energy and, as a consequence, the inelastic collisions become unimportant. Finally, the bimodal distribution is an estimate of an EEDF that takes into account the strong electric fields in the cathode sheath. It is composed by the superposition of a beam of electrons, provided by a normal distribution—to account for those electrons that have not experienced a collision—with an equilibrium distribution, either a Boltzmann or a Druyvesteyn, of electrons, to account for those electrons that have experienced collisions. Variations in the average energy, shape, and the fraction of the total electron population in the electron beam would account for changes in spatial location and operating conditions.

Simulation Results and Discussion

Tables 2 and 3 compare the results using the Maxwell-Boltzmann, Druyvesteyn, and bimodal distributions of different energies. Model parameters used in the simulation are shown in Table 4. The species concentrations are reported as a fraction of the total ionization. The base case (no electron beam) in Table 2 is a Maxwell-Boltzmann distribution at a thermal temperature kT of 5 eV (1 eV = 1.6×10^{-19} J) corresponding to an average energy, $3/2\ kT$, of 7.5 eV, while the base case in Table 3 is a Druyvesteyn distribution at an average energy of 10 eV. The 30% increase in average energy for the Druyvesteyn distribution was required to maintain the same level of ionization (a common

Table 3. Results Obtained with Different Druyvesteyn Electron Beam Bimodal Distributions

kT, eV	6.7	6.7	6.7	6.7	6.7	6.7	6.7	6.7
Fraction normal beam	0.0	0.15	0.15	0.15	0.15	0.15	0.15	0.15
Beam average energy, eV	0.0	10.0	12.5	13.5	15.0	17.0	19.0	20.0
Net average energy, eV	10.0	10.0	10.4	10.5	10.75	11.0	11.4	11.5
Fractional ionization $\times 10^3$	3.8	1.6	1.6	1.6	1.7	2.0	3.6	7.2
H, as fraction of TI*	4.28	3.69	4.95	5.29	5.10	5.0	5.2	5.40
H^-, as fraction of TI*	0.17	0.08	0.08	0.08	0.08	0.10	0.20	0.31
H_2^+, as fraction of TI*	0.20	0.19	0.19	0.19	0.19	0.19	0.19	0.20
H_3^+, as fraction of TI*	0.63	0.73	0.73	0.73	0.73	0.71	0.61	0.49

*TI = total ionization

Table 4. Model Parameters

Average ion energy	1 eV
Average neutral energy	0.025 eV
Pressure	0.67 Pa (5 mTorr)
Volume/area of reactor	2×10^{-2} M

characteristic in our comparison) as with a MB distribution. This can be understood by examining Figure 2 and observing that at the same average energy (7.5 eV) roughly an order of magnitude fewer electrons are in the high-energy tail (i.e., above the ionization threshold energy) of the Druyvesteyn distribution than in the high-energy tail of the MB distribution. Thus, an increase in average energy is required to achieve the same electron population above the threshold energy and consequently the same fractional ionization.

The other significant difference between the MB and Druyvesteyn base cases is the fraction of hydrogen atoms produced. Consider the Druyvesteyn distribution at an average energy of 10 eV as shown in Figure 2. The lower population of electrons in the high-energy tail of the Druyvesteyn distribution is counterbalanced by a similar lower population of electrons at low energies. The combined effect is a surplus of electrons at energies greater than the dissociation threshold energy, but less than the ionization threshold energy of the hydrogen molecule. This results in a 50% increase in the concentration of hydrogen atoms relative to the concentration of hydrogen ions for the Druyvesteyn distribution, as compared to the MB distribution.

Similar effects are observed when an electron beam is introduced. At low average beam energies the beam does not have a high fraction of electrons above the ionization threshold. Even though the average energy of the combined EEDF may increase, the fraction of electrons available for ionization decreases and so does the fractional ionization. As the beam energy is increased, but maintained below the ionization threshold energy, the fraction of hydrogen atoms increases while the ionization remains approximately constant. For beam energies above the ionization threshold energy, the fractional ionization again increases but the relative fraction of hydrogen atoms decreases. At sufficiently high beam energies above the dissociative ionization threshold energy, both ionization and dissociation increase rapidly. Thus, as the electron beam energy is increased, the reactions are sequentially promoted one by one in order of increasing threshold energies.

The results from this simple simulation support the empirical notion that the EEDF can play a major role in the reaction kinetics of a plasma-assisted reactor. The total ionization and thus the production of reactive species in a plasma depends on the number density of electrons with energies greater than the threshold energies and not simply on the average energy of the EEDF. Moreover, the relative steady state concentrations of the species in the plasma are affected by the shape of the EEDF. Thus, simply putting more energy into the plasma may not give the optimum reactor performance. In order to fully exploit the dependence of reaction rates on the EEDF, plasma process simulations need to be developed which account for the effect of the operating conditions on the EEDF and thus, the corresponding effect on the reaction kinetics. Only then can a rational design of plasma reactors for deposition and etching be accomplished.

Acknowledgment

This work was funded by a grant from the University of Delaware Research Foundation.

Notation

A = surface area of reactor walls
$E_{th,j}$ = threshold energy for reaction j
$f_i(\rho v, r, t)$ = energy distribution function of species i
$f_i(\epsilon)$ = collision energy distribution function for reaction i
k_j = rate constant for reaction j
$k_{loss,i}$ = rate constant for species i to reactor walls
kT_i = thermal temperature of species i
m_i = atomic mass of species i
n_i = number density of species i
r = position vector
r_j = rate of reaction j
t = time
v = velocity vector
V = reactor volume
$x_{i,j}$ = net stoichiometric coefficient of species i in reaction j
$Y_{e,i}$ = net charge of species i
$y_{H,i}$ = number of H atoms in species i
$z_{i,j}$ = reactant stoichiometric coefficient of species i in reaction j

Greek letters

γ_i = empirical correction factor for loss of species i
ϵ = collision energy
σ_j = collision cross section of reaction j
τ_i = kinetic transition time for species i

Subscripts

i = species index (H, H_2, H^+, H_2^+, H_3^+, e)
j = reaction index

Superscript

0 = initial condition

Literature Cited

Boeuf, J. P., and E. Marode, "A Monte Carlo Analysis of an Electron Swarm in a Nonuniform Field: The Cathode Region of a Glow Discharge in Helium," *J. Phys. D: Appl. Phys.*, **15**, 2169 (1982).

Boswell, R. W., and I. J. Morey, "Self-consistent Simulation of a Parallel-plate RF Discharge," *Appl. Phys. Lett.*, **53**(1), 21 (1987).

Boyd, R. L. F., and N. D. Twiddy, "Electron Energy Distributions in Plasmas: I," *Proc. R. Soc.*, **A250**, 53 (1959).

Capitelli, M., R. Celiberto, C. Gorse, R. Winkler, and J. Wilhelm, "Electron Energy Distribution Function in He-CO Radio Frequency Plasmas: The Role of Vibrational and Electronic Superelastic Collisions," *J. Appl. Phys.* **62**(11), 4398 (1987).

Capitelli, M., C. Gorse, R. Winkler, and J. Wilhelm, "On the Modulation of the Electron Energy Distribution Function in Radio Frequency SiH_4, SiH_4-H_2 Bulk Plasmas," *Plasma Chem. Plasma Proc.* **8**(4), 399 (1988).

Chung, P. H., L. Talbot, and K. J. Touryon, *Electric Probes in Stationary and Flowing Plasmas: Theory and Application,* Springer. New York, (1975).

Cox, T. I., V. G. I. Deshmukh, D. A. O. Hope, A. J. Hydes, N. St. J. Braithwaite and N. M. P. Benjamin, "The Use of Langmuir Probes and Optical Emission Spectroscopy to Measure Electron Energy Distribution Functions in RF-Generated Argon Plasmas," *J. Phys. D: Appl. Phys.*, **20**, 820 (1987).

Deshmukh, V. G. I., and T. I. Cox, "Physical Characterization of Dry Etching Plasmas Used In Semiconductor Fabrication," *Plasma Phys. Controlled Fusion,* **30**(1), 21 (1988).

Ferreira, C. M., and J. Loureiro, "Electron Excitation Rates and Transport Parameters in High-Frequency N_2 Discharges," *J. Phys. D: Appl. Phys.*, **22**, 76 (1988).

Fukumasa, O., R. Itatani, and S. Saeki, "Numerical Simulation of Hydrogen Ion Species in the Steady-State Plasma of a Low-Pressure Ion Source," *J. Phys. D: Appl. Phys.*, **18**, 2433 (1985).

Graves, D. B., and K. F. Jensen, "A Continuum Model of DC and RF Discharges," *IEEE Trans. Plasma Sci.*, **PS-14**(2), 78 (1986).

Janev, R. K., W. D. Langer, K. Evans, Jr., and D. E. Post, Jr., *Elementary Processes in Hydrogen–Helium Plasmas*, Springer (1987).

Kline, L. E., and M. J. Kushner, "Computer Simulation of Materials Processing Plasma Discharges," *Crit. Rev. Solid State Matl. Sci.*, **16**, 1 (1989).

Kline, L. E., W. D. Partlow, and W. E. Bies, "Electron and Chemical Kinetics in Methane RF Glow-discharge Plasmas," *J. Appl. Phys.*, **65**, 70 (1989).

Kushner, M. J., "Monte Carlo Simulation of Electron Properties in RF Parallel-Plate Capacitively Coupled Discharges, *J. Appl. Phys.*, **54**(9), 4958 (1983).

———, "A Model for the Discharge Kinetics and Plasma Chemistry During Plasma-Enhanced Chemical Vapor Deposition of Amorphous Silicon," *J. Appl. Phys.*, **63**(8), 2532 (1988).

Loureiro, J., and C. M. Ferreira, "Electron Excitation Rates and Transport Parameters in Direct-Current N_2 Discharges," *J. Phys. D: Appl. Phys.*, **22**, 67 (1989).

Ohuchi, M., and T. Kubota, "Monte Carlo Simulation of Electrons in the Cathode Region of the Glow Discharge of Helium," *J. Phys. D: Appl. Phys.*, **16**, 1705 (1983).

Shirai, H., and K. Tabei, "Non-Maxwell Electron Energy Distribution and Radiation of Nonequilibrium Nitrogen Plasmas," *Trans. Japan Soc. Aero. Space Sci.*, **29**(84), 89 (1986).

Sommerer, T. J., W. N. G. Hitchon, and J. E. Lawler, "Electron Heating Mechanisms in Helium RF Glow Discharges: A Self-consistent Kinetic Calculation," *Phys. Rev. Lett.*, **63**(21), 2361 (1989).

Venugopalan, M., *Reactions Under Plasma Conditions*, Wiley-Interscience, New York (1971).

Wani, K., "Evaluation of the Electron Energy Distribution in a Low-pressure Hg–Ar Discharge with a Two-temperature Approximation," *J. Appl. Phys.*, **63**(12), 5683 (1988).

Wertheimer, M. R., and M. Moisan, "Comparison of Microwave and Lower Frequency Plasmas for Thin Film Deposition and Etching," *J. Vac. Sci. Technol. A*, **3**(6), 2443 (1985).

Manuscript received June 14, 1990, and revision received July 16, 1990.